https://doi.org/ 10.33472/AFJBS.6.8.2024.1-22

African Journal of Biological Sciences

Numerical investigation of MHD micropolar nanofluids with impacts of Viscous Dissipation and Radiation over an inclined permeable stretching surface

T. Lokesh Babu[1*], S.V.H.N. Krishna Kumari[2] and MN Raja Shekar[3]

[1]Department of Mathematics, Sreenidhi Institute of Science and Technology, Hyderabad, Telangana, India

[2]Department of Mathematics, Aurora Deemed to be university,Hyderabad, Telangana, India

3Department of Mathematics, JNTUH UCESTH, Hyderabad, Telangana, India

Article History
Volume 6,Issue 8, Feb 2024
Received:01 Mar 2024
Accepted : 28 Mar 2024
doi: 10.33472/AFJBS.6.8.2024.1-22

Abstract

In this study, we model the free convective flow of a micropolar fluid with electrical conductivity between a porous material and a permeable stretched sheet. Fluid behaviour under the impact of certain constituent factors has been the subject of many different study by researchers around the globe, with some very interesting and unique conclusions emerging from these studies. Little is known about how Viscous Dissipation interacts with micropolar nanofluid flow over a slanted stretching surface. The ordinary differential equations are derived from the governing partial differential equations by using an appropriate equivalent substitution. The numerical solutions to these sophisticated nonlinear coupled equations are more involved, hence computational solutions, like the MATLAB inbuilt solver bvp4c, are used instead. The behaviour of factors that describe the flow phenomenon is shown on graphical representations, and the calculated values of physical qualities that are important can be viewed in the form of tables.

Keywords: Micropolar nanofluid, Eckert number, Stretching surface, porous media, bvp4c.

Introduction

Due to their growing importance and practical relevance in numerous manufacturing procedures, non-Newtonian fluids have recently attracted a lot of interest from scientists and engineers studying mechanics. Non-Newtonian fluids have diverse scientific and technological

uses, including polymer technology, fuel drilling, processing food, and many more. A property of micropolar liquids is the presence of microconstituents, that have the ability to spin within the atoms of the fluid and impact the flow's hydrodynamics. When submerged in a slightly sticky liquid, potential distortions might be difficult to detect due to the presence of hard, arbitrarily pointed elements with microstructural elements. Their symmetrical motion and the existence of exactly symmetric solutions are equivalent to those of the standard Navier-Stokes equation; however, the former is not necessarily realizable, which is why the Buongiorno model must be used. Because of this, micropolar fluids are preferred in industrial operations for using in paints, polymeric liquids, solutions with colloidal particles, and other similar products.

Kim[1] investigated the heat and mass transfer that occurs in MHD micropolar flow across a moving permeable plate that is vertical in a medium that is porous.Micropolar fluids in MHD) flow approaching a vertical surface stagnation point were explored by Ishak et al. [2]. Micropolar fluids approaching stagnation points and moving towards non-linear stretch surfaces were studied by Hayat et al. [3] in terms of their MHD flow. In their study, Khedr et al. [4] investigated the micropolar fluid's MHD flow via a stretched porous surface that might generate or absorb heat. When it comes to micropolar fluid flow via a vertical porous material, Islam et al. [5] get into the details. Extensive research on fully established convective micropolar fluid stream in erect channels with slip was conducted by Ashmawy [6]. An investigation on the stagnation point flow of a micropolar fluid across a stretching/shrinking layer with 2nd velocity slip was carried out by Sharma et al. for the purpose of [7]. Heat transfer and the movement of a micropolar fluid via a porous stretched sheet were studied by Turkyilmazoglu [8]. Ibrahim[9] investigated the micropolar fluid's heat exchange and boundary layer motion through a stretching sheet with slip in a MHD circumstance. The flow of micropolar fluids in a porous substance subjected to different slip circumstances was studied by Fatunmbi et al. [10]. A study by Yasmin et al.[11] looked at the mass and heat exchange in multi-homogeneous fluid flow over an elongated stretched sheet. Goud et al. [12] investigated the impact of Ohmic heating, chemical reaction on micropolar fluids MHD flow via a stretched surface. The impact of velocity slip on micropolar liquid MHD flow on a surface that is stretching was investigated by Pattnaik et al. [13].

When it comes to studying boundary layer flows, the stretching situation is crucial because of the amazing results it has in various engineering and industrial applications, such as paper and wire drawing, polymer engineering, hot rolling, plastic sheet extraction, metal bed cooling, glass formation, and many more. The field of convective thermal transfer in nanofluids has lately made significant strides in understanding and improving a range of manufacturing operations. The thermal efficiency of nanofluids has been the subject of a great deal of scientific and theoretical exploration. The flow going through a stretched plate was investigated by Crane [14]. An exponentially extending surface was the subject of Nadeem's [15] investigation of the boundary layer flow of nanofluid. Using a solution for analysis, Hassani [16] investigated the flow of a nanofluid via an extensible sheet in the boundary layer. For their study, Ibrahim and Shanker [17] used a convective surface boundary circumstance to examine the nanofluid's boundary-layer movement and transfer of heat across a vertical plate. Through the use of an increasingly stretched surface, Nadeem and Leee[18] investigated how boundary layer flow of nanofluid. Under the influence of a permeable elastic sheet with a convection boundary

circumstance, Malvandi et al. [19] investigated the boundary layer's impact on slip and the transfer of heat of nanofluid. The simulated work by Mabood et al. [20] looked into the flow of tiny fluids over a nonlinear stretching surface and the heat transmission in the MHD interface layer. An analysis on MHD boundary layer flow rotating framing nanofluid with chemical responses is explored by Dharmaiah et al. [21]. Within the perspective of a nanofluid with dissipation, Zulkifli [22] conducted an investigation into a numerical model of flow across the boundary layer over a moving surface. Using a numerical simulation, Ferdows et al. [23] investigated the constant nanofluid boundary layer movement across a moving plate while simultaneously generating heat and suction.

Due to its numerous engineering and manufacturing uses, including heat exchange systems, food production, geothermal power recovery, developing the insulation, flow via filtering gadgets, air conditioning and filters processes, etc., the transmission of heat and mass examination on a surface embedded within a material that is porous has recently drawn the interest of scientists and engineers. Over the past few decades, researchers have examined convection mass and heat transfer in porous media in a number of experiments.

Heat and mass transmission in porous media were some of the topics investigated by Dagan [24].The buoyancy impact of free convection in a porous media with coupled heat and mass transport were studied by Trevisan and Adrian [25]. For their study, Das et al. [26] used oscillatory suction and a heat source to investigate the outcomes of mass transfer on MHD flow as well as heat transmission via a porous material via a vertically oriented plate. Unsteady multi-layer hydrodynamic free convective heat transfer and flow through a vertical porous plate subjected to changing suction and internal heat production were investigated by Sharma & Singh [27]. In the instance of an influenced by heat the source, Ravikumar et al.[28] investigated the influence of the transfer of mass and heat on multi-homogeneous hydrodynamic flow (MHFD) of a viscous fluid via a non-homogeneous media that is porous. The heat and mass transport in a mixed convection flow with moving inclined permeable plates was studied by Raju et al. [29]. some impacts were all factors that Manglesh and Gorla [30] considered while studying MHD free convective motion in porous media. The continuous flow of a convective fluid via a porous plate in its occurrence of numerous factors was investigated by Mopuri et al. [31] in their MHD transfer of mass and heat study.

Considering the reviews of literature that have been listed above, as well as the increasing demand for micropolar nanofluids in the science and technology and industrial sectors, we have been motivated to conduct a numerical analysis of the flow problem of micropolar nanofluids MHD flow through a stretching sheet that includes a heat source and a chemical reaction. In order to attain the numerical result, the built-in solver bvp4c of Matlab was used. Additionally, the influence of a number of different physical factors was explored both numerically and visually.

Mathematical formulation

The hydromagnetic flow of nanofluids that possess micropolar properties with respect to a permeable stretched surface that is inclined at an angle γ. In this context, 'x' represents the position of the object in the path of the stretching surface, and 'a' is a constant. The velocities that are taken into consideration are $u_w(x) = ax$ and $u_\infty(x) = 0$ at the wall and far away

from the wall, respectively. The transverse magnetic field is assumed to be at a right angle to the extending surface. This expectation is based on the idea that the impacts of the electric and magnetic fields are insignificant due to the short magnetic Reynolds number.

At the same time as they collide with another particle and spin in the fluid fields, the micropolar and nanoparticle that make up the particles of the fluid are freely disseminated throughout the base fluids. These particles are of a limited size. C_w *and* T_w are constant values for the nanoparticle fraction and temperature, respectively, with C_∞ and T_∞ representing the mass fraction and temperature at the wall and far away from the wall, correspondingly. The values of C_w and T_w respectively are constant. The flow geometry is shown in the following figure, which is referred to as Fig.1.

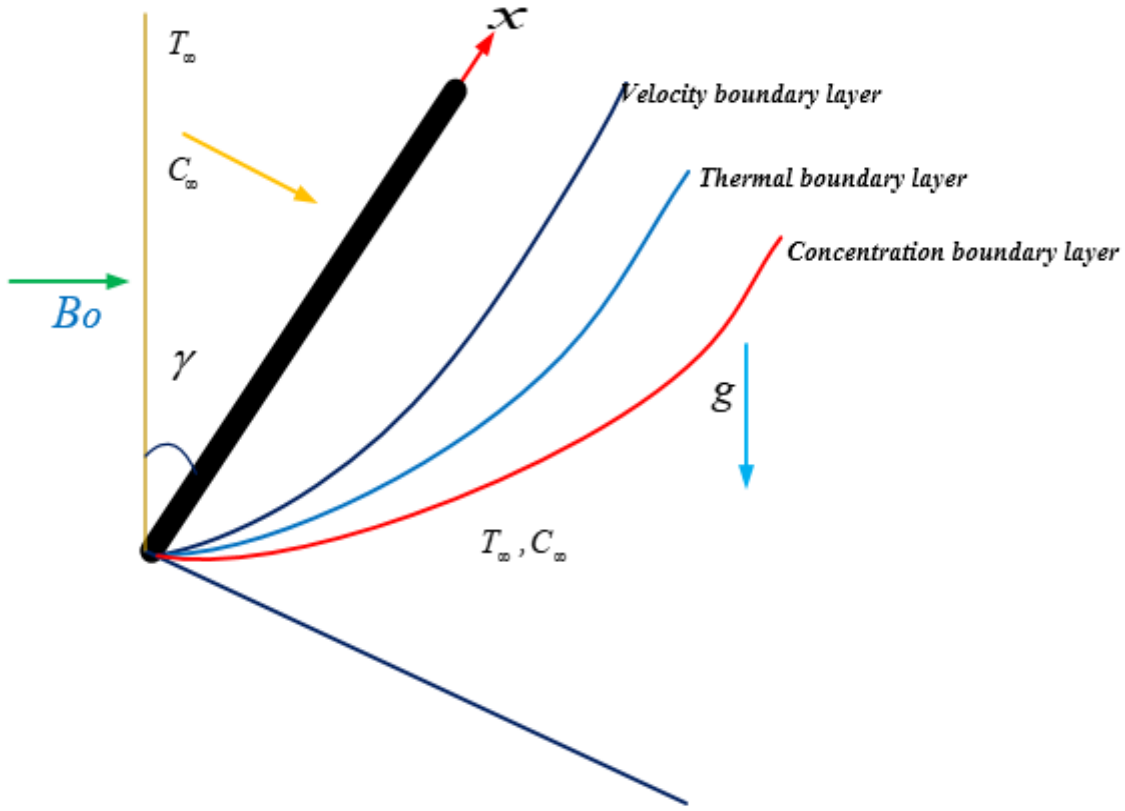

Fig. 1: Flow geometry .

A representation of the flow's governing equations may be found below:

$$\frac{\partial u}{\partial x}+\frac{\partial v}{\partial y}=0 \quad (1)$$

$$u\frac{\partial u}{\partial x}+v\frac{\partial u}{\partial y}=\left(\frac{\mu+K_1^*}{\rho}\right)\frac{\partial^2 u}{\partial y^2}+\left(\frac{K_1^*}{\rho}\right)\frac{\partial N^*}{\partial y}+g\beta_T(T-T_\infty)cos\gamma+g\beta_c(C-C_\infty)cos\gamma-\left(\frac{\sigma B_0^2}{\rho}\right)u-\frac{v^*}{K_1^*}u \quad (2)$$

$$u\frac{\partial N^*}{\partial x}+v\frac{\partial N^*}{\partial y}=\left(\frac{\gamma^*}{j^*\rho}\right)\frac{\partial^2 N^*}{\partial y^2}+\left(\frac{K_1^*}{j^*\rho}\right)\left(2N^*+\frac{\partial u}{\partial y}\right) \quad (3)$$

$$u\frac{\partial T}{\partial x}+v\frac{\partial T}{\partial y}=\alpha\frac{\partial^2 T}{\partial y^2}+\tau\left(D_B\frac{\partial T}{\partial y}\frac{\partial C}{\partial y}+\frac{D_T}{T_\infty}\left(\frac{\partial T}{\partial y}\right)^2\right)-\frac{1}{\rho C_p}\frac{\partial q_r}{\partial y}+\frac{Q_0}{\rho c_p}(T-T_\infty)+\left(\frac{\mu+K_1^*}{\rho C_p}\right)\left(\frac{\partial u}{\partial y}\right)^2+\left(\frac{\sigma B_0^2}{\rho C_p}\right)u^2 \quad (4)$$

$$u\frac{\partial C}{\partial x}+v\frac{\partial C}{\partial y}=\tau\left(D_B\frac{\partial^2 C}{\partial y^2}+\frac{D_T}{T_\infty}\frac{\partial^2 T}{\partial y^2}\right)-K_r^*(C-C_\infty) \quad (5)$$

The following is a list of the boundary circumstances:

$$\left.\begin{array}{ll} u=u_w(x)=ax, v=V_wN^*=-m\frac{\partial u}{\partial y}, T=T_w, C=C_w & at\ y=0 \\ u\to u_\infty(x)=0, v\to 0, N^*\to 0,, T\to T_\infty, C\to C_\infty & at\ y\to\infty \end{array}\right\} \quad (6)$$

Taking $\psi = \psi(x,y)$ as stream function, where $u=\frac{\partial\psi}{\partial y}$ and $v=-\frac{\partial\psi}{\partial y}$ (7)

Equation (1) is fulfilled in the same accurate manner. For the changes to take place, the following is required:

$$\left.\begin{array}{c} \zeta=y\sqrt{\frac{a}{\upsilon}}, N^*=ax\sqrt{\frac{a}{\upsilon}}\ h(\zeta), \theta(\zeta)=\frac{T-T_\infty}{T_w-T_\infty}, \phi(\zeta)=\frac{C-C_\infty}{C_w-C_\infty} \\ u=axf'(\zeta), v=-\sqrt{av}f(\zeta) \end{array}\right\} \quad (8)$$

By putting Equation (8) into the set of equations (2)–(5), we would be able to derive the following:

$$(1+K)f'''+ff''-f'^2-(M+Kp)f'+Kh'+(Gr\theta+Gc\phi)\cos\gamma=0 \quad (9)$$

$$\left(1+\frac{K}{2}\right)h''+fh'-f'h-K(2h+f'')=0 \quad (10)$$

$$\left(\frac{1+R}{Pr}\right)\theta''+Q\theta+f\theta'+Nb\theta'\phi'+Nt\,\theta'^2+(1+K)Ecf''+EcMf'^2=0 \quad (11)$$

$$\phi''+Lef\phi'-KrLe\phi+\left(\frac{Nt}{Nb}\right)\theta''=0 \quad (12)$$

A few additional substitutes that were included in equations (9–12) were able to be obtained by us from the dimensionless components that are given below.

$$\left.\begin{array}{c} M=\frac{\sigma B_0^2}{a\rho}, Le=\frac{\upsilon}{D_B}, k=\frac{k_1^*}{\mu}, Pr=\frac{\upsilon}{\alpha}, Q=\frac{Q_0}{\alpha\rho C_p}, K=\frac{K_1^*}{\mu}, Kr=\frac{v^*}{K_r^*a}, \\ Ec=\frac{u_w^2}{Cp(T_w-T_\infty)}, \alpha=\alpha^*\mu\sqrt{\frac{a}{v}}, Re_x=\frac{u_w(x)x}{\upsilon}, R=\frac{16\sigma^*T_\infty^3}{3\rho C_p}, \alpha=\frac{k}{\rho C_p}, \\ \tau=\frac{(\rho C_p)_p}{(\rho C_p)_f}, Nb=\frac{\tau D_T(T_w-T_\infty)}{\upsilon T_\infty}, Gr=\frac{g\beta_T(T_w-T_\infty)}{xa^2}, Gr=\frac{g\beta_C(C_w-C_\infty)}{xa^2}, \\ fw=-\sqrt{av}\,V_w \end{array}\right\} \quad (13)$$

The following are the changed boundary the circumstances:

$$\left.\begin{array}{c} f=fw, f=1+\alpha(1+K)f'', h=-mf'', \theta=1, \phi=1\ \ at\ \ \zeta=0 \\ f'\to 0,\ \ h\to 0,\ \ \theta\to 0,\ \ \phi\to 0, \qquad as \qquad \zeta\to\infty \end{array}\right\} \quad (14)$$

At the surface, shear stress, heat and mass flux specified as,

$$\tau_w=\left[(\mu+k)\left(\frac{\partial u}{\partial\zeta}\right)+kN\right]_{\zeta=0}=(\mu+k)ax\sqrt{\frac{b}{v}}f''(0), q_w(x)=-k_f\left(\frac{\partial N}{\partial\zeta}\right)_{\zeta=0}=$$

$$-k_f(T_w-T_\infty)\sqrt{\frac{b}{v}}\,\theta'(0)\,, J_w=-D\left(\frac{\partial C}{\partial\zeta}\right)_{\zeta=0}$$

And Friction factor, couple stress, Nusselt number and Sherwood number specified ad

$$C_f=\frac{\tau_w}{\rho u_w^2}=\frac{(1+K)f''(0)}{\sqrt{Re_w}},\ M_w=\left(\gamma\frac{\partial N}{\partial\zeta}\right)_{\zeta=0}=\mu u_w\left(1+\frac{k}{2}\right)h'(0),\ \ Nu_x=\frac{xh(x)}{k_f}=-\sqrt{\frac{a}{v}}x\theta'(0)$$

and written as $\frac{Nu_x}{\sqrt{Re_w}}=-\theta'(0)$, $Sh_x=\frac{J_w(x)}{D(C_w-C_\infty)}=-\sqrt{\frac{b}{v}x}\phi'(0)$ and it provides

$-\phi'(0)=\frac{Sh_x}{\sqrt{Re_w}}$.

METHOD OF SOLUTION

A solution can be obtained by converting the set of non-linear ODEs. (9)–(12) with boundary conditions (14) into an IVP. We made $y_1 = f, y_2 = f', y_3 = f'', y_4 = g, y_5 = g', y_6 = \theta, y_7 = \theta', y_8 = \phi, y_9 = \phi'$ subsequent transformation of the ODEs into below form:

$$y'_3 = -(y_1 * y_3 - (y_2)^2 - (M + Kp) * y_2 + (K * y_5) + (Gr * y_6 + Gc * y_8)cos\gamma)/(1 + K)$$

$$y'_5 = -((y_1 * y_5) - (y_2 * y_4) - (K * (2 * y_4 + y_3)))/\left(1 + \frac{K}{2}\right)$$

$$y'_7 = -(\left((y_1 * y_7) + (1 + K)Ecy_3 + MEc(y_2)^2\right) + Nby_7y_9 + Nt(y_7)^2)/(1 + R)$$

$$y'_9 = -Le(y_1 * y_9) + LeKry_8 - \frac{Nt}{Nb}y_7$$

Boundary restrictions consist of

$$\left.\begin{array}{l} y_1(0) = f_w, y_2(0) = 1 + \alpha(1 + K)y_3, y_4(0) = -my_3(0), y_6(0) = 1, y_8(0) = 1 \\ y_2(\infty) = 0, y_4(\infty) = ,0\ y_6(\infty) = 0, y_8(\infty) = 0 \end{array}\right\}$$

In order to integrate the resulting differential equations, one may subsequently employ the solver technique integrated into MATLAB. The preceding method is repeated until the outcomes attain the necessary level of precision 10^{-6}.

Code Validation

An examination of the fluctuation of the Nusselt number (0) for various Prandtl number values with previous research is presented in Table 1. It is evident from the table that our findings are highly consistent with those reported by Hassani et al. [32], Makinde, and Aziz [33] under limiting circumstances. In addition, in order to verify the precision of the numerical options, an examination of the transfer rates for various Pr values is conducted with Abdul-Kahar et al. [34], with whom an excellent concurrence is observed.

Table 1: A comparison of the outcomes for the Nusselt number $-\theta'(0)$.

Pr	Hassani et al.[32]	Makinde and Aziz[33]	Abdul-Kahar et al.[34]	Present study
0.7	0.4582	0.4539	0.454285	0.4543
2	0.9114	0.9114	0.911423	0.9114
7	1.8956	1.8954	0.895264	0.8952
20	3.3539	3.3539	3.353853	3.3538

Results and Discussion

The primary aim of the present inquiry is to illustrate how various physical parameters affect the pattern of flow along the available stretched sheet. In addition to the boundary circumstances (14), equations (9–12) are computationally computed. Consequently, the acquired numbers are depicted through the use of figures and tables.

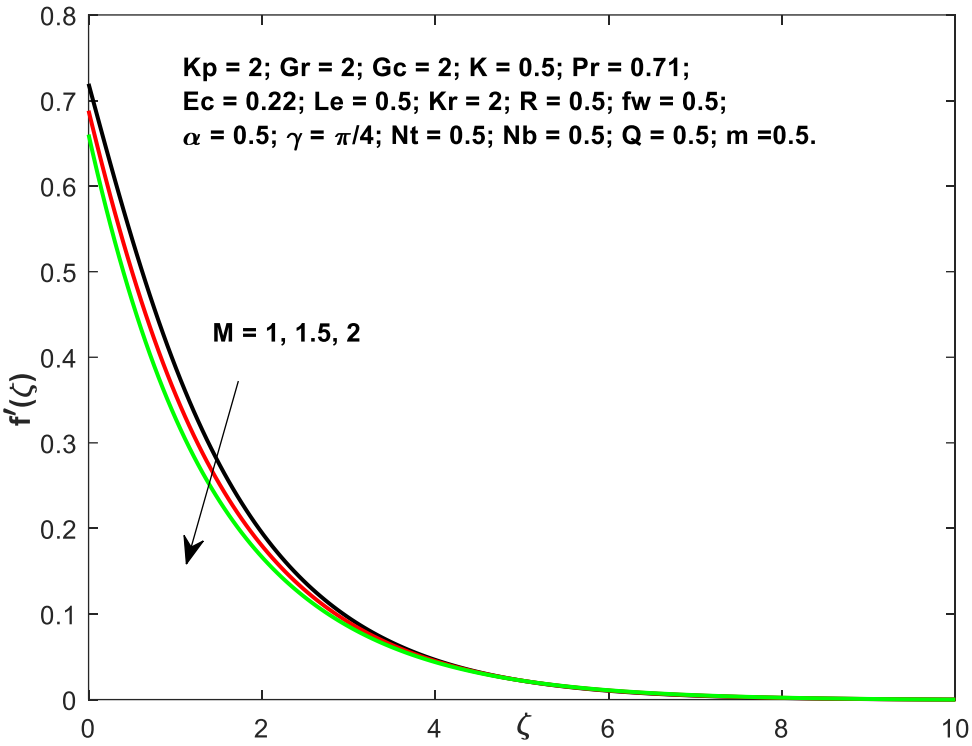

Fig.2: M vs $f'(\zeta)$.

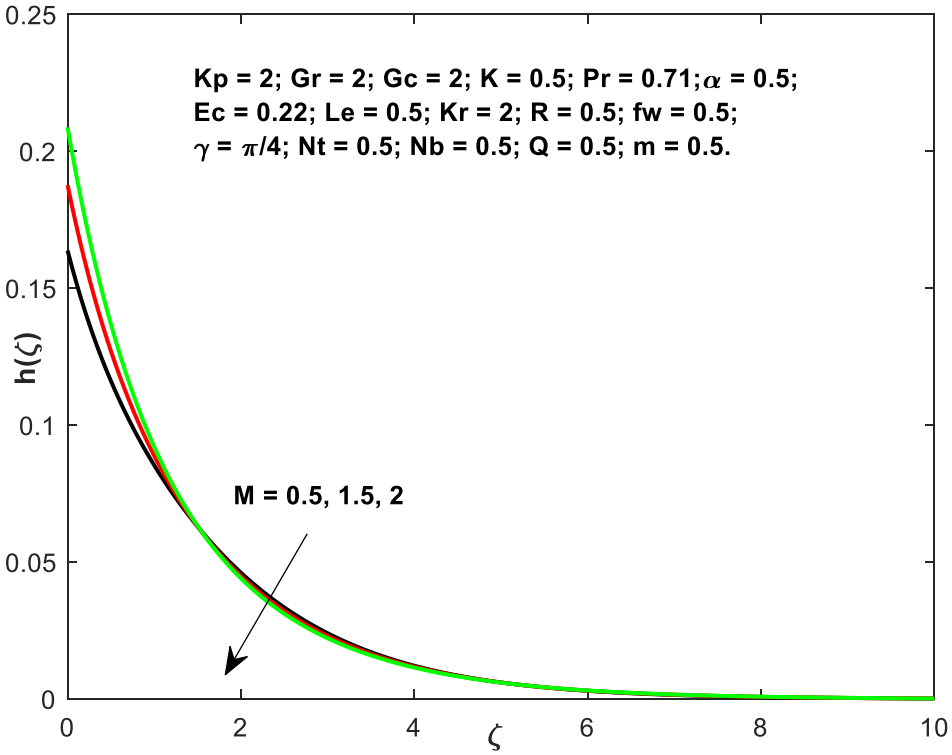

Fig.3: M vs $H(\zeta)$.

The impact of magnetic parameter variations on velocity and microrotation patterns is illustrated in Figures 2 and 3, respectively. M. The Lorentz force, which opposes the momentum of particles in fluids, is generated as a result of the magnetic field. As illustrated in Figure 1, the sheet experiences a displacement of the velocity border layer as an outcome of

the Lorentz force. Based on the rising values of the magnetic variable, Figure 3 illustrates how the microrotation curves decrease asymptotically until they reach the boundary layer. Primarily, the Lorentz force, which impedes the fluid velocity, is accountable for the decrease in microrotation patterns.

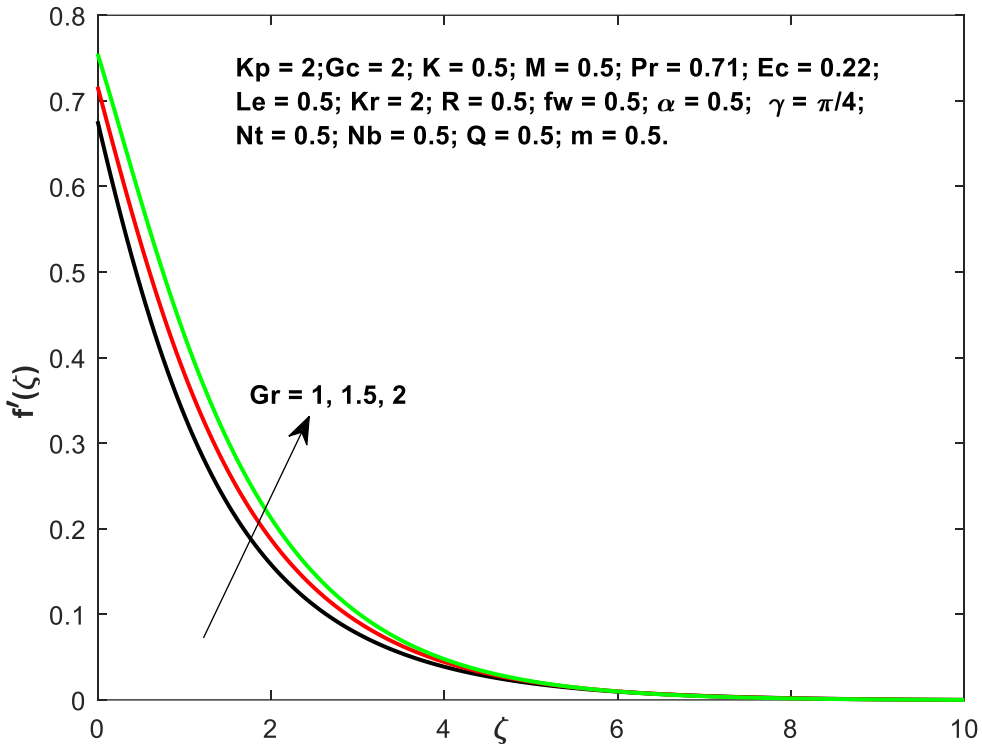

Fig. 4: Gr vs $f'(\zeta)$.

An assortment of thermal Glasof number Gr values are represented in Figure 4, which illustrates the fluctuation of velocity. The increase in thermal buoyancy force results in a steady acceleration of the object, as anticipated.

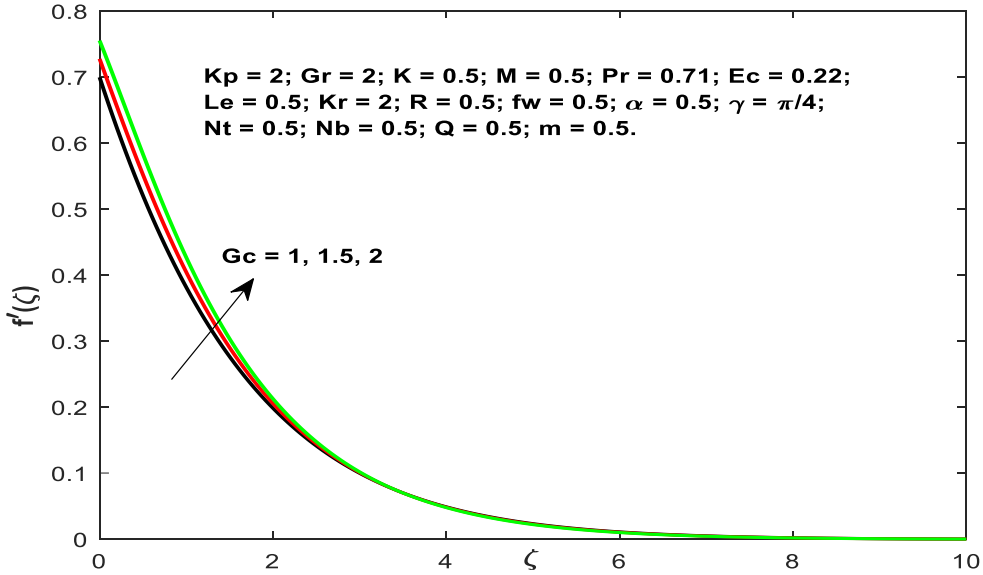

Fig.5: Gc vs $f'(\zeta)$.

Figure 5 illustrates the fluctuation of velocity across multiple sets of values of the solute Grashof number Gc. As anticipated, the species buoyant force causes a rise in fluid velocity, resulting in a more pronounced peak value.

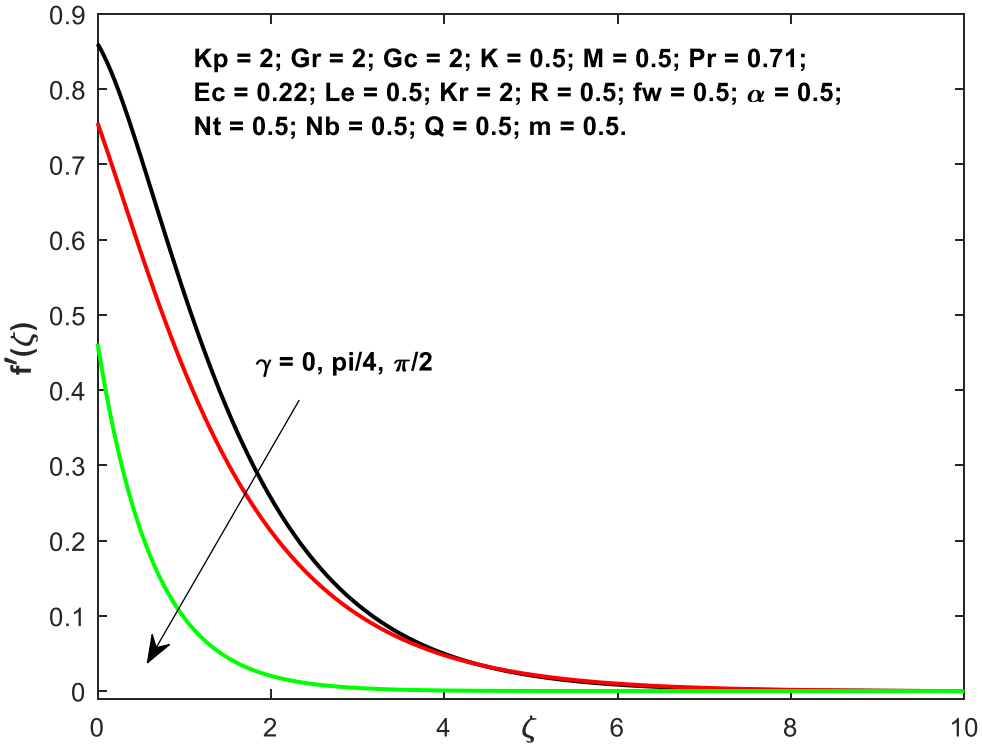

Fig.6: γ vs $f'(\zeta)$.

The velocity distribution declines as the inclination factor γ upsurges, as shown in Figure 6. This corresponds to a decrease in the bouncy force amplitude as the inclination parameter increases by a factor of Cosγ due to temperature fluctuation.

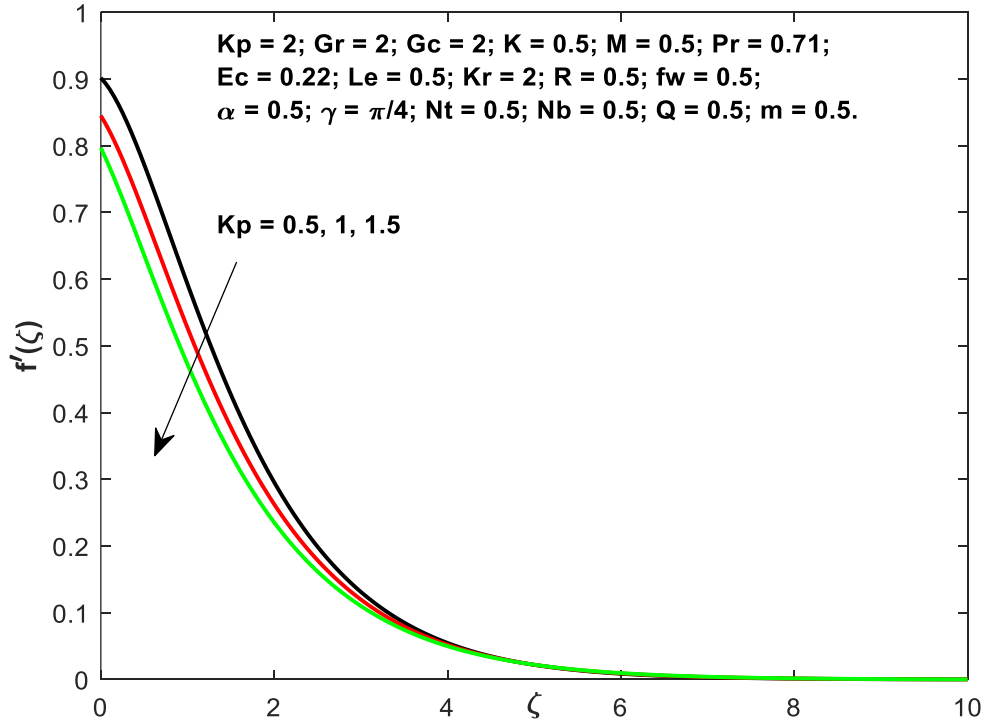

Fig.7: Kp vs$f'(\zeta)$.

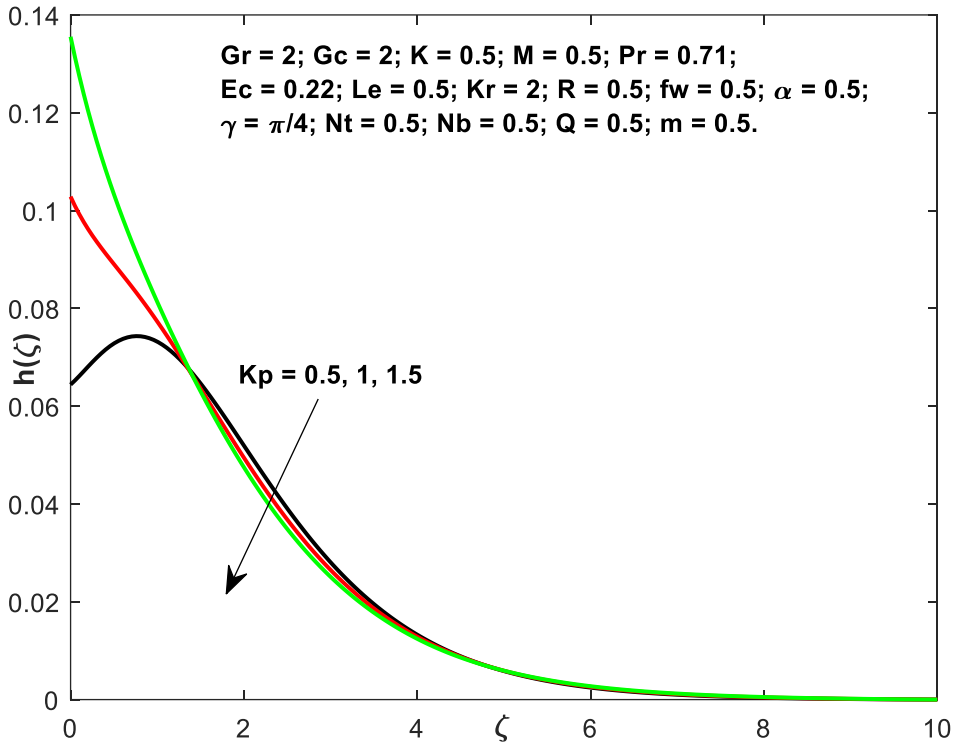

Fig.8: Kp vs $h(\zeta)$.

Figs.7-8 show how the porosity parameter, Kp, affects velocity, microrotation, and profile. As seen in Fig.7, the flow stream reductions as the parameter values of the porous media improve. A lesser permeability parameter might result in a greater Darcian resistance to the flow of fluid, since the momentum equation shows that the Darcian resistance force is inversely proportional to the permeability parameter. A rising value of Kp results in a smaller flow field. In addition, Fig.8 shows that the profiles of microrotation are minimized.

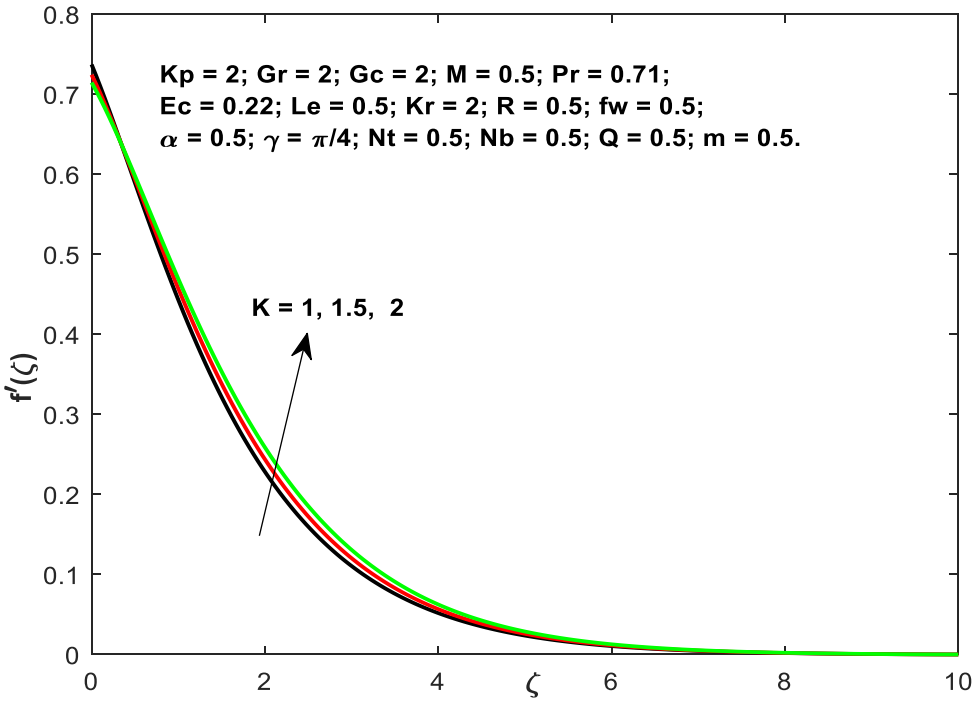

Fig.9: K vs $f'(\zeta)$.

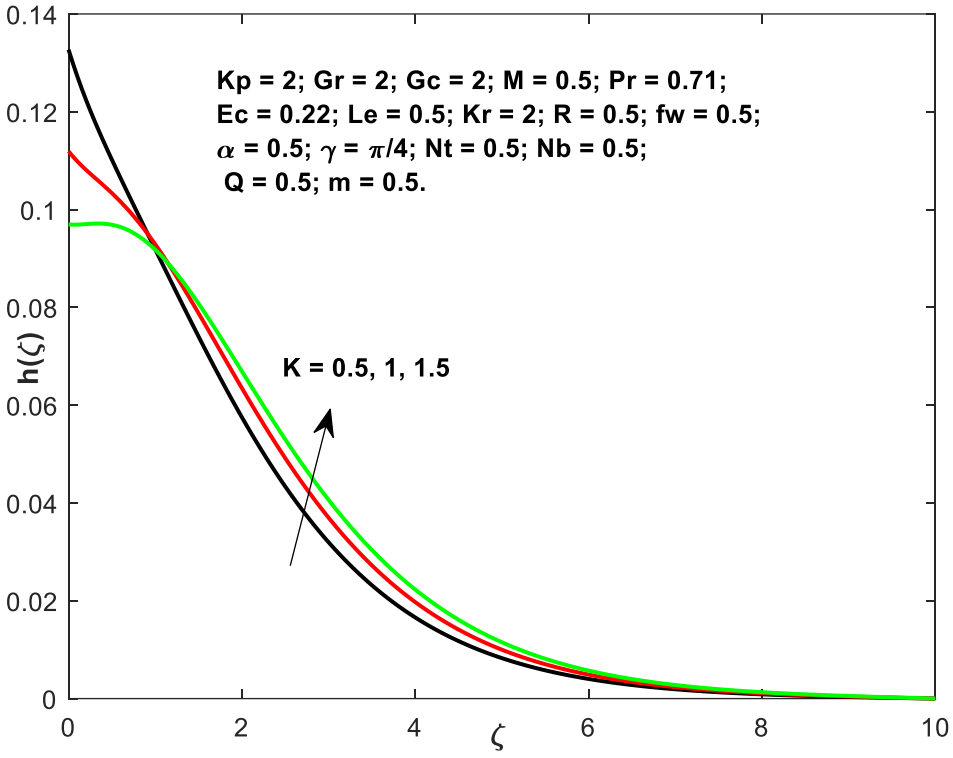

Fig.10: K vs $h(\zeta)$.

Results for velocity and micro rotation profile as a function of material parameter (K) are shown in Figures 9 and 10. The velocity and microrotation curves improve as K values rise. According to physical principles, the micropolar fluidity factor is the material property that may change the velocity distribution of micropolar fluids.

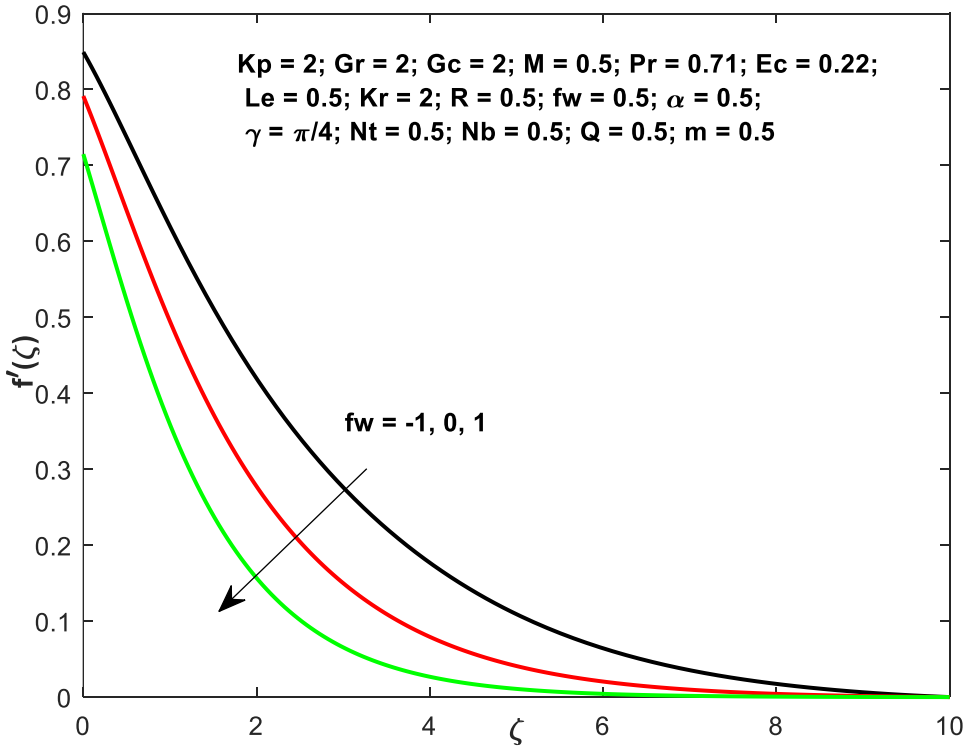

Fig.11: fw vs $f'(\zeta)$.

Fig.11 demonstrate the plots of velocity, microrotation, and temperature as a function of the suction/injection a. It shows how changing the value of an impacts the velocity. Both the suction/injection velocity distributions show a diminishing relationship with increasing.

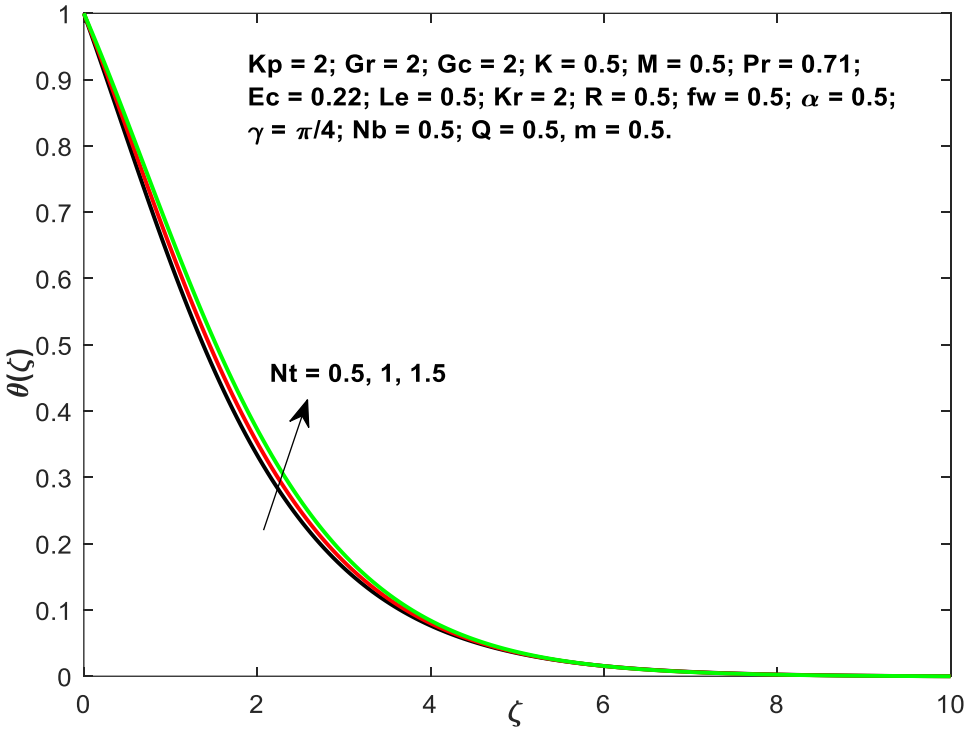

Fig.12: Nt vs $\theta(\zeta)$.

The impact of this factor on the temperature fluctuation is seen in Fig.12. The presence of nanoparticles in the base fluid that react to a temperature difference indicates the existence of a thermophoretic impact. With a rise in the thermophoretic impact, nanoparticles migrate deeper from the heated sheet to the surrounding fluid, which is cold. Due to this an enhance in Nt causes the thermal boundary layer to expand.

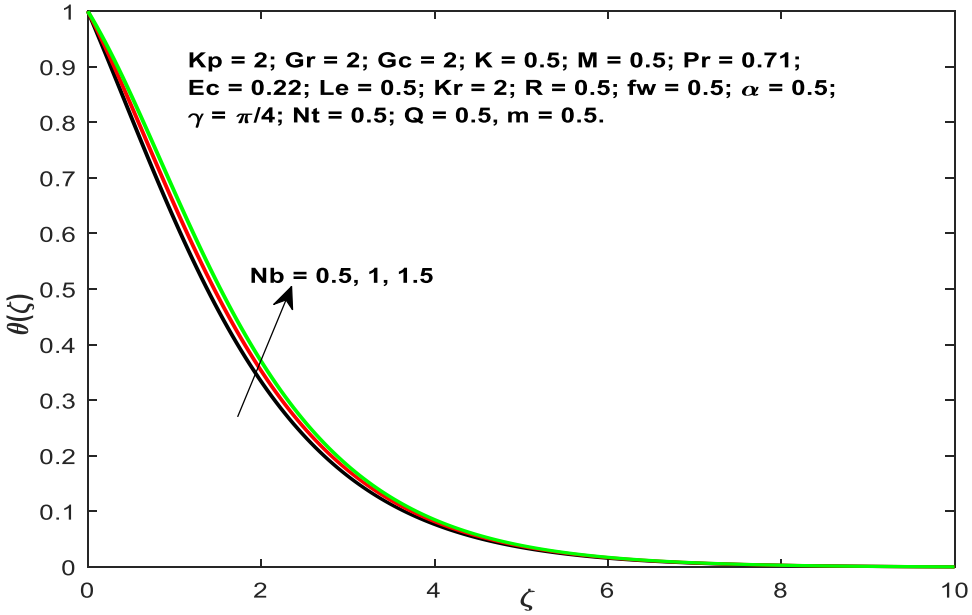

Fig.13: Nb vs $\theta(\zeta)$.

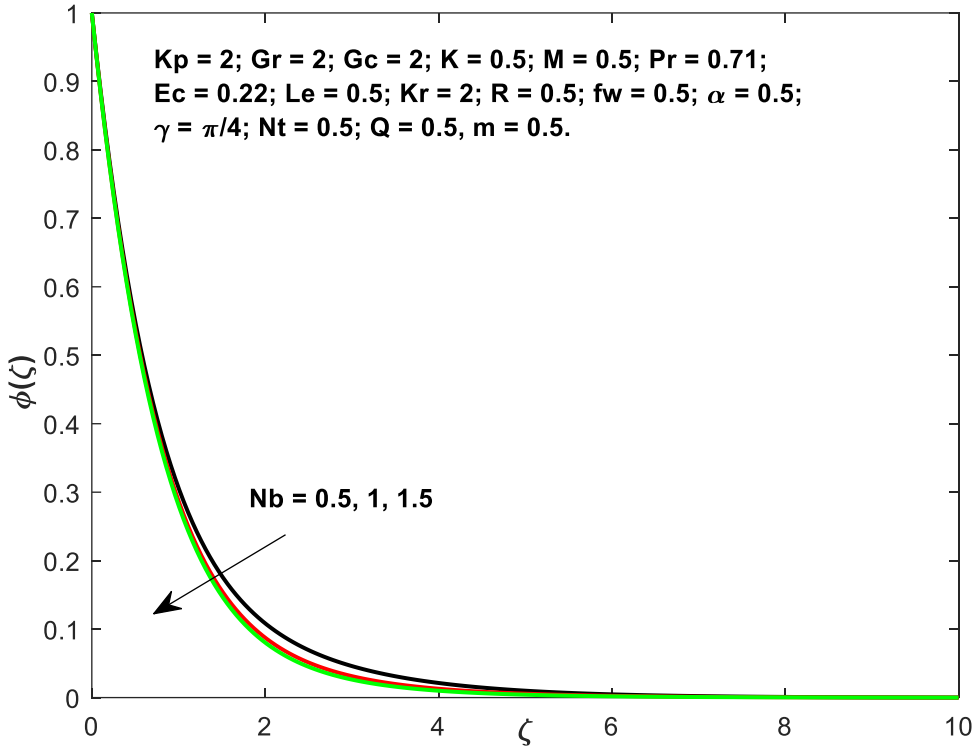

Fig.14: Nb vs $\phi(\zeta)$.

The effect of Brownian motion on concentration gradients is shown in Fig.13, while the impact on temperature profiles is shown in Fig.14. Raising the temperature and decreasing the concentration are the results of improving the Brownian motion factor. Because nanoparticles travel with a degree of unpredictability and irregularity brought about by Brownian motion, the rate of impacts within the flow rises, leading to a heating of the thermal barrier layer. Because of this, the concentration profile drops.

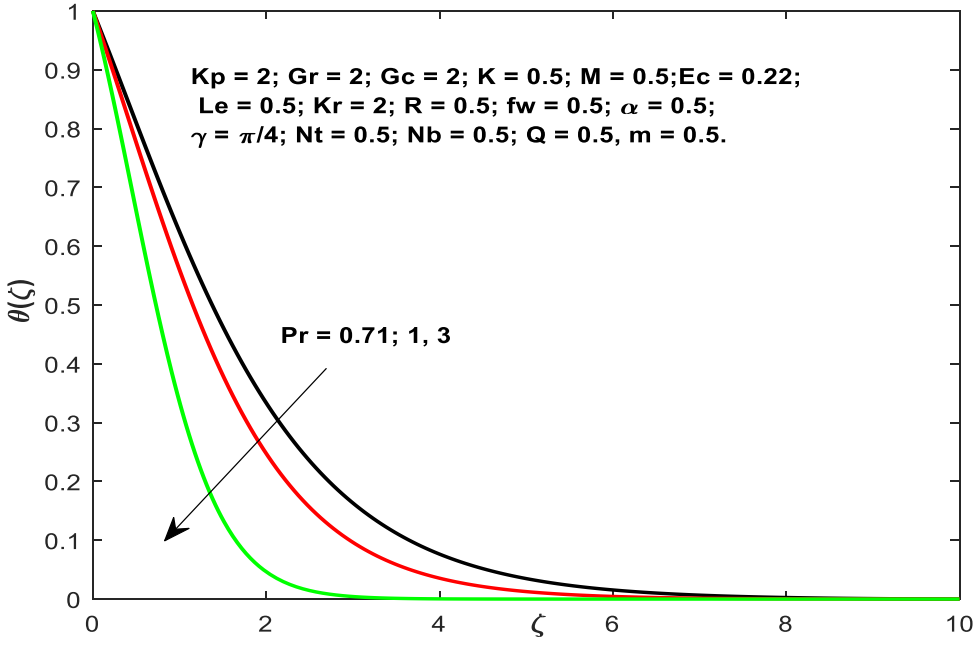

Fig.15: Pr vs $\theta(\zeta)$.

Fig.15 shows that the heat transfer gradients get less steep as Pr number becomes higher. This is because a faster rate of heat diffusion away from the heated surface is achieved when Pr values is increased, which is comparable to a decrease in thermal conductivity. The result is a decrease in heat transmission and a thinner boundary layer as the Pr values increases.

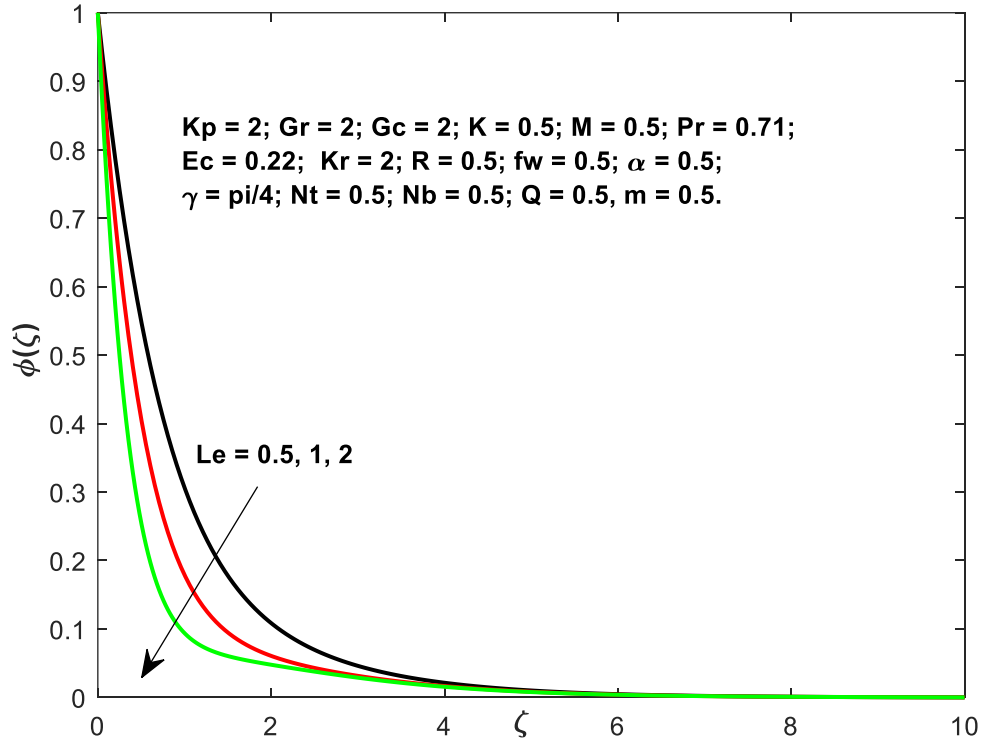

Fig.16: Le vs $\phi(\zeta)$.

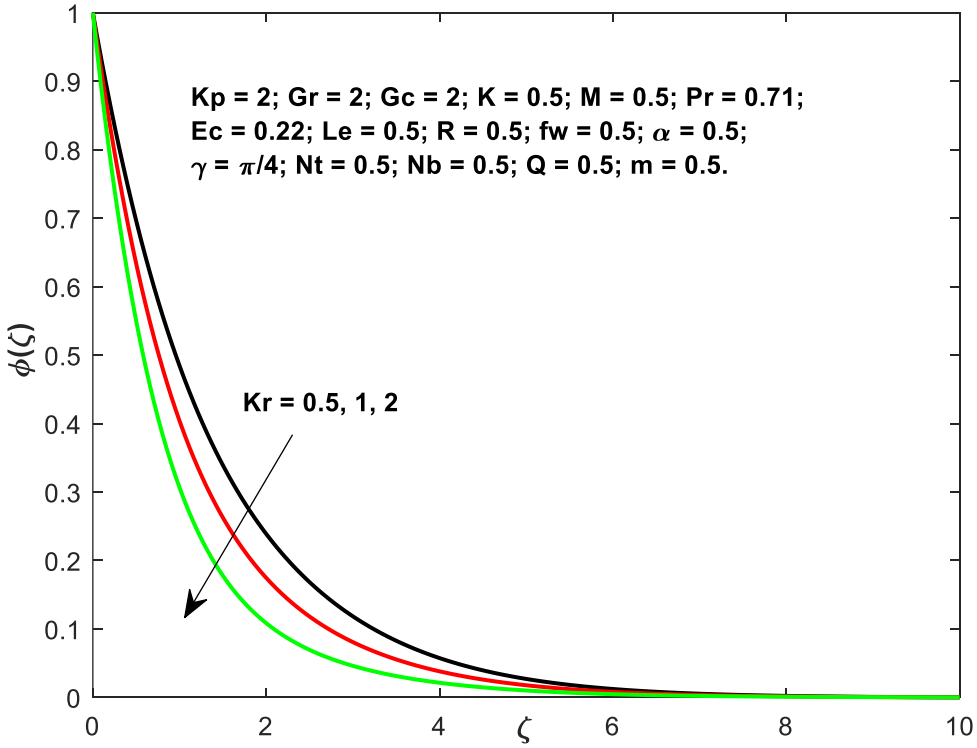

Fig.17: Kr vs $\phi(\zeta)$.

Fig.16 shows the concentration characteristic of the micropolare fluid as a function of the Lewis number, whereas Fig.17 shows the same profile for chemical reaction factors. The concentration profile reduced significantly in response to small changes in the Lewis number. Consequently, the micropolare distribution limit has diminished dramatically can see in Fig. 16. Fig.17 shows how the concentration gradient is affected by the chemical reaction factor(Kr). The concentration curve has reduced as Kr has been increased. It should be noted that the concentration layer has grown in size as Kr factor has increased.

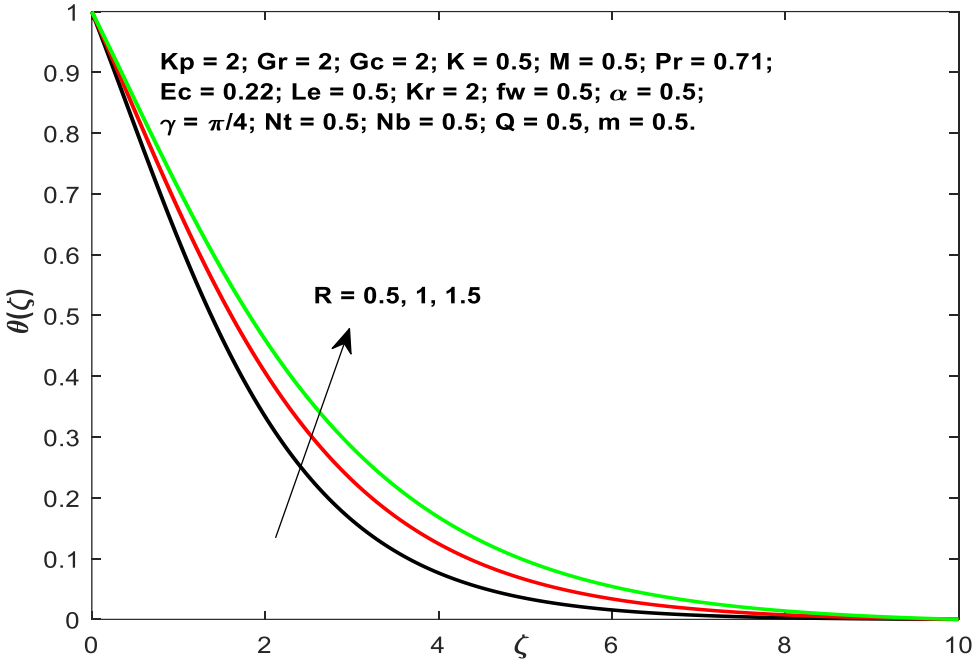

Fig.18: R vs $\theta(\zeta)$.

Figure 18 shows the temperature gradients with every other variable held constant, along with the impact of R. It can be detected from this diagram that as R upsurges, both the temperature field and the width of the thermal boundary layer goes up.

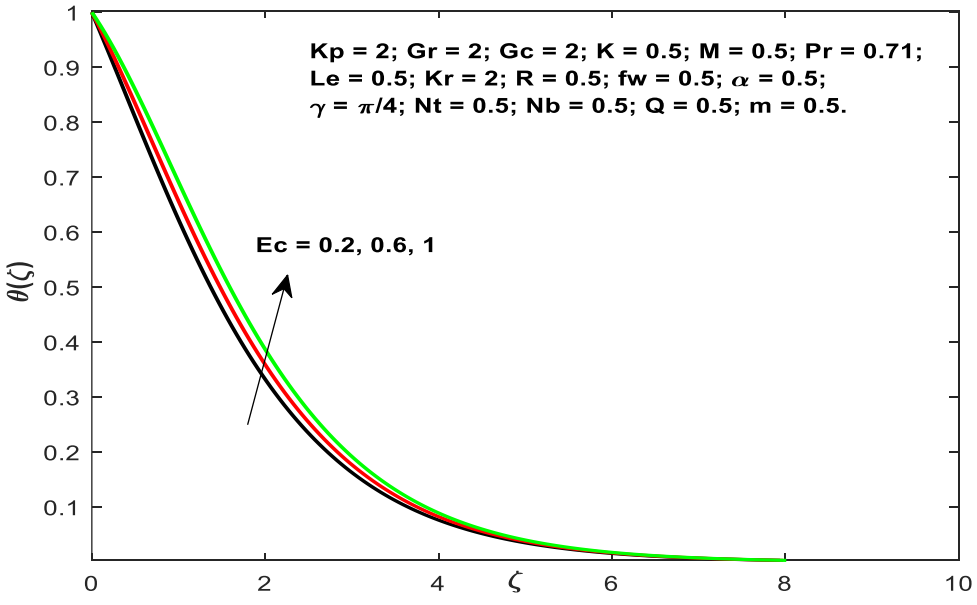

Fig.19: Ec vs $\theta(\zeta)$.

The influence of the viscous dissipation variable, namely the Eckert number Ec, on the temperature gradients is seen in Figure 19. An object's Eckert number indicates the amount of mechanical energy that is dissipated as heat as a result of internal friction. Consequently, the system will get hotter as the Ec values rise because more thermal energy will be added to the flow. A higher Eckert number is associated with much higher temperatures.

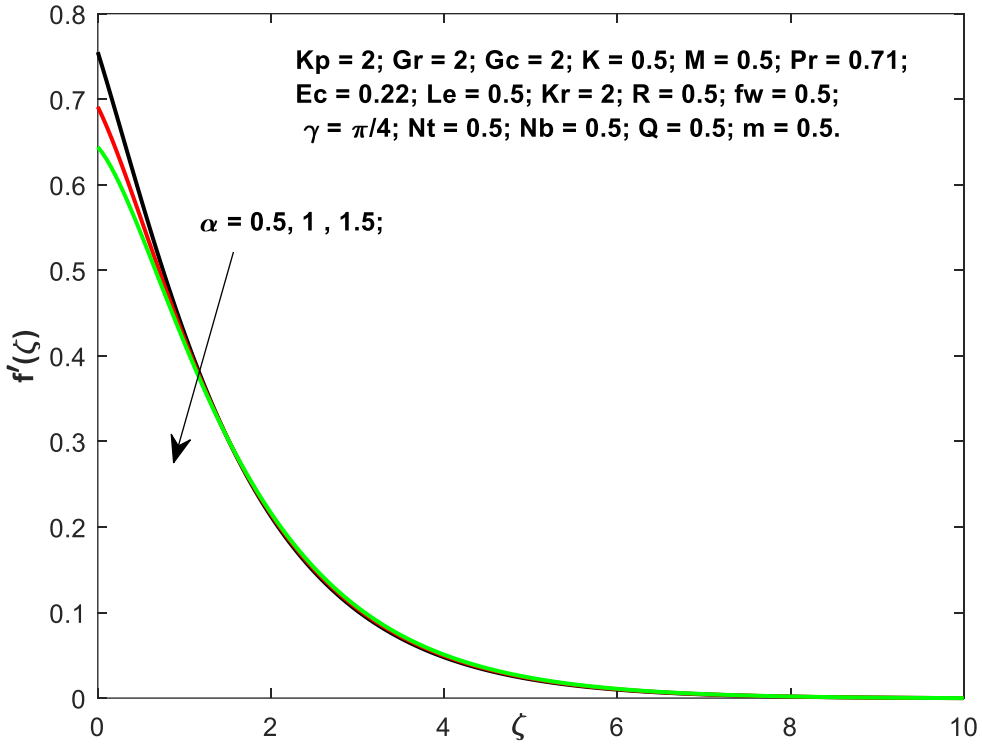

Fig.20: α vs $f'(\zeta)$.

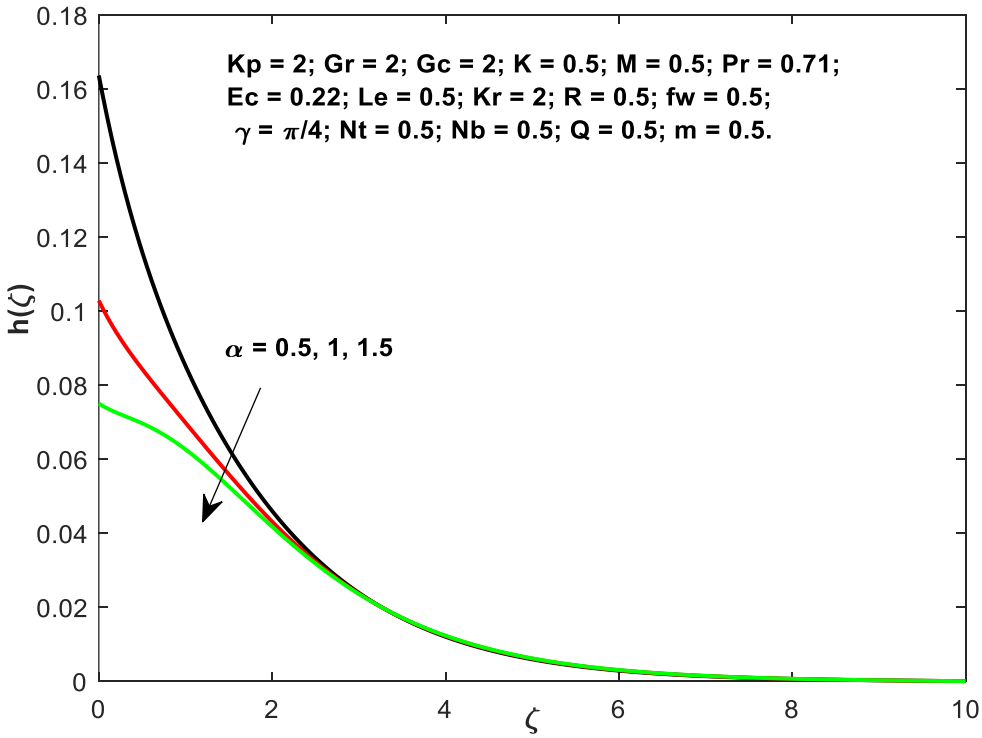

Fig.21: α vs $h(\zeta)$.

Figures 20 and 21 show how f' and h change as the slip parameter (α) is varied.By examining the profiles, one can see that the velocity and microrotation patterns are diminished when the slip parameter is increased.

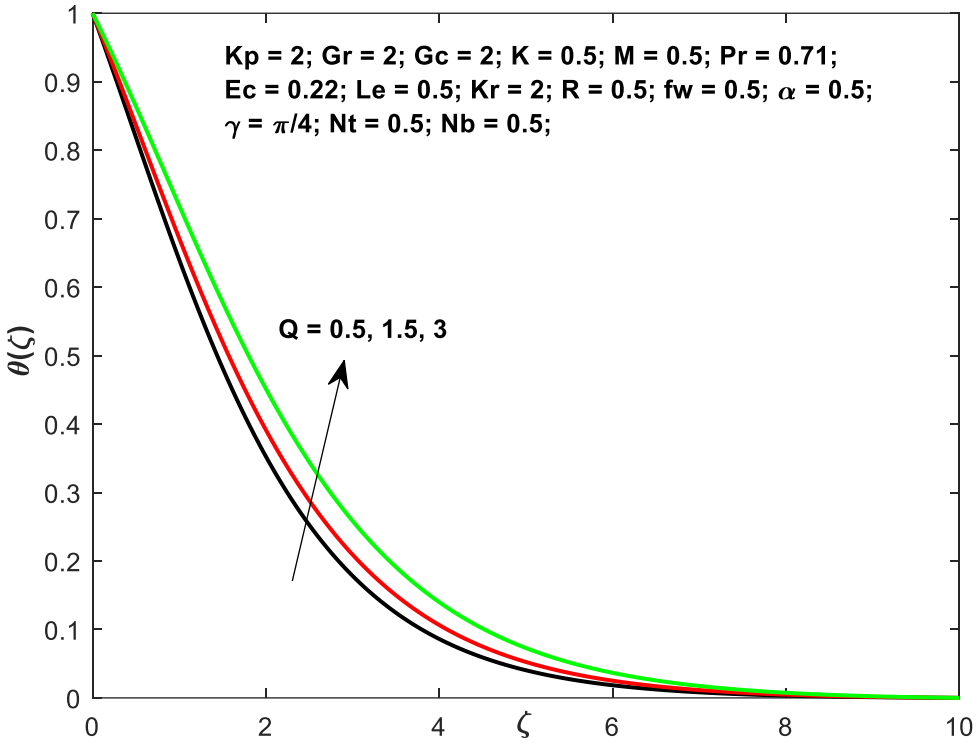

Fig.22: Q vs $\theta(\zeta)$.

The impact on the temperature distribution curves with varying values of the parameter γ, while the other variables were held constant, is shown in Figure 22. The image shows that when the internal heat production parameter Q> 0 is stronger, the temperature gradient gets wider, whereas the converse is true for the heat absorption factor Q < 0. Additionally, it should be noted that the boundary layer fluid temperature distribution was found to be maximum when the heat production parameter, Q, was greater than zero. Similarly, it is shown that a decrease in the temperature gradient is caused by the impact of Q< 0, as the heat extracted from the sheet is reduced.

A list of the numerical values of, $(1+K)f''(0)$, $\left(1+\frac{k}{2}\right)h'(0)$, $-\theta'(0)$, and $-\phi'(0)$ can be found in Table 2. We observe that an increase in M *and* Kp leads to an increase in the skin-friction and Sherwood number, while the Nusselet number and the wall couple stress decreases. When the fw was raised, there was a drop in wall couple stress, but there was a rise in skin friction, Nusselet number, and Sherwood number. When γ increases the skinfriction upsearges and reverse impact in other field. In Table 3, the numerical values of the aforementioned parameters have been shown for a variety of relevant parameters. There is a possibility that the rate of heat transfer drops as the rises Ec Nt, Nb, Le Kr and R, although the opposite effect has been seen for the Sherwood number,opposite trend is seen with Pr

Table 2. Numerical values of $(1+K)f''(0), \left(1+\frac{k}{2}\right)h'(0), -\theta'(0)$, and $-\phi'(0)$ with $K = 0.5; Pr = 0.71; Ec = 0.22; Le = 0.5; Kr = 2; R = 0.5;\ A = 0.5;\ Q = 0.5; Gr = 2;\ Gc = 2; Nt = 0.5;\ Nb = 0.5;\ m = 0.5;$

M	fw	Kp	γ	$(1+K)f''(0)$	$\left(1+\frac{k}{2}\right)h'(0)$	$-\theta'(0).$	$-\phi'(0)$
0.5	0.5	2	$\pi/4$	0.490841	0.969126	0.328127	1.201075
1				0.562518	0.961174	0.298101	1.204535
1.5				0.625713	0.954335	0.273274	1.206953
0.5	1			0.574927	0.952341	0.464779	1.298999
	0			0.415596	0.980196	0.211331	1.098748
	-1			0.297682	0.991071	0.049672	0.887311
	0.5	3		0.627891	0.954228	0.302172	1.196075
		4		0.734794	0.943076	0.280605	1.192528
		2	$\pi/3$	0.650756	0.951712	0.298089	1.195280
			$\pi/2$	1.08495.0	0.914559	0.17004	1.184613

Table 3: Numerical values of $-\theta'(0)$ and $-\phi'(0)$ with $K = 0.5; M = 0.5; Kr = 2; R = 0.5;\ fw = 0.5;\ A = 0.5;\ Kp = 2;\ Q = 0.5; Gr = 2;\ Gc = 2; \gamma = \pi/4;\ m = 0.5;$

Pr	Ec	Nt	Nb	Le	Kr	R	$-\theta'(0).$	$-\phi'(0)$
0.71	0.22	0.5	0.5	0.5	2	0.5	0.328127	1.201075
1							0.375117	1.194426
3							0.473893	1.192641
	0.4						0.297665	1.212181
	0.6						0.263593	1.224567
		0.7					0.315186	1.200829
		0.9					0.302771	1.203330
			0.7				0.304280	1.211938
			0.9				0.282283	1.217704
			0.5	1			0.312895	1.810587
				3			0.297350	3.634289
					3		0.320402	1.420437
					4		0.315216	1.606287
						0.7	0.311108	1.203490
						0.9	0.296291	1.205567

Conclusions

Due to the significance of the micropolar fluid including nanoparticles when it comes to the heat transfer process in sectors as well as cooling systems, the present research is an effort to analyze the flow behavior of the micropolar fluid via a stretched sheet. Following are the results that were obtained from the study:

- Larger values of M, α, γ, Kp and fw decreases the velocity profile whereas it increase with Gr, Gc, K.
- Microrotation declines for higher values of M, α and Kp and upsurge for K.
- Temperature increases for the enhanced values of $Ec, Nt, Nb, R$and Q, while it decreases with increase of Pr,
- Concentration drops with the enhanced values of Le, Nb and Kr.
- The skin-friction and Sherwood numbers are raised by M and Kp, but there is a decrease in both the Nusselt number and the wall couple stress.
- Nusselt number drops as the rises $Ec\ Nt, Nb, Le\ Kr$ and R, although the reverse consequence has been seen for the Sherwood number.

References

1. Kim, Youn J. "Heat and mass transfer in MHD micropolar flow over a vertical moving porous plate in a porous medium." Transport in Porous Media 56 (2004): 17-37.
2. Ishak, Anuar, Roslinda Nazar, and Ioan Pop. "Magnetohydrodynamic (MHD) flow of a micropolar fluid towards a stagnation point on a vertical surface." Computers & Mathematics with Applications 56, no. 12 (2008): 3188-3194.
3. Hayat, T., T. Javed, and Z. Abbas. "MHD flow of a micropolar fluid near a stagnation-point towards a non-linear stretching surface." Nonlinear Analysis: Real World Applications 10, no. 3 (2009): 1514-1526.
4. Khedr, M-EMM, A. J. J. Chamkha, and M. Bayomi. "MHD flow of a micropolar fluid past a stretched permeable surface with heat generation or absorption." Nonlinear Analysis: Modelling and Control 14, no. 1 (2009): 27-40.
5. Islam, Ariful, Md Haider Ali Biswas, Md Rizaul Islam, and S. M. Mohiuddin. "MHD micropolar fluid flow through vertical porous medium." Academic research international 1, no. 3 (2011): 381.
6. Ashmawy, E. A. "Fully developed natural convective micropolar fluid flow in a vertical channel with slip." Journal of the Egyptian Mathematical Society 23, no. 3 (2015): 563-567.
7. Sharma, Rajesh, Anuar Ishak, and Ioan Pop. "Stagnation point flow of a micropolar fluid over a stretching/shrinking sheet with second-order velocity slip." Journal of Aerospace Engineering 29, no. 5 (2016): 04016025.
8. Turkyilmazoglu, M. "Flow of a micropolar fluid due to a porous stretching sheet and heat transfer." International Journal of Non-Linear Mechanics 83 (2016): 59-64.
9. Ibrahim, Wubshet. "MHD boundary layer flow and heat transfer of micropolar fluid past a stretching sheet with second order slip." Journal of the Brazilian Society of Mechanical Sciences and Engineering 39, no. 3 (2017): 791-799.
10. Fatunmbi, Ephesus Olusoji, Hammed Abiodun Ogunseye, and Precious Sibanda. "Magnetohydrodynamic micropolar fluid flow in a porous medium with multiple slip conditions." International Communications in Heat and Mass Transfer 115 (2020): 104577.

11. Yasmin, Asia, Kashif Ali, and Muhammad Ashraf. "Study of heat and mass transfer in MHD flow of micropolar fluid over a curved stretching sheet." Scientific reports 10, no. 1 (2020): 4581.
12. Goud, B. Shankar, and Mahantesh M. Nandeppanavar. "Ohmic heating and chemical reaction effect on MHD flow of micropolar fluid past a stretching surface." Partial Differential Equations in Applied Mathematics 4 (2021): 100104.
13. Pattnaik, P. K., D. K. Moapatra, and S. R. Mishra. "Influence of velocity slip on the MHD flow of a micropolar fluid over a stretching surface." In Recent Trends in Applied Mathematics: Select Proceedings of AMSE 2019, pp. 307-321. Springer Singapore, 2021.
14. Crane, Lawrence J. "Flow past a stretching plate." Zeitschrift für angewandte Mathematik und Physik ZAMP 21 (1970): 645-647.
15. Nadeem, Sohail, and Changhoon Lee. "Boundary layer flow of nanofluid over an exponentially stretching surface." Nanoscale research letters 7 (2012): 1-6.
16. Hassani, M., M. Mohammad Tabar, H. Nemati, G. Domairry, and F. Noori. "An analytical solution for boundary layer flow of a nanofluid past a stretching sheet." International Journal of Thermal Sciences 50, no. 11 (2011): 2256-2263.
17. Ibrahim, Wubshet, and Bandari Shanker. "Boundary-layer flow and heat transfer of nanofluid over a vertical plate with convective surface boundary condition." (2012): 081203.
18. Nadeem, Sohail, and Changhoon Lee. "Boundary layer flow of nanofluid over an exponentially stretching surface." Nanoscale research letters 7 (2012): 1-6.
19. Malvandi, A., F. Hedayati, and D. D. Ganji. "Boundary layer slip flow and heat transfer of nanofluid induced by a permeable stretching sheet with convective boundary condition." Journal of Applied Fluid Mechanics 8, no. 1 (2014): 151-158.
20. Mabood, Fazle, W. A. Khan, and AI Md Ismail. "MHD boundary layer flow and heat transfer of nanofluids over a nonlinear stretching sheet: a numerical study." Journal of Magnetism and Magnetic Materials 374 (2015): 569-576.
21. Dharmaiah, G., N. Vedavathi, K. S. Balamurugan, and K. Ramakrishna. "A study on MHD boundary layer flow rotating frame nanofluid with chemical reaction." Frontiers in Heat and Mass Transfer (FHMT) 12 (2018).
22. Zulkifli, Siti Norfatihah, Norhafizah Md Sarif, and Mohd Zuki Salleh. "Numerical solution of boundary layer flow over a moving plate in a nanofluid with viscous dissipation: A revised model." Journal of Advanced Research in Fluid Mechanics and Thermal Sciences 56, no. 2 (2019): 287-295.
23. Ferdows, M., M. D. Shamshuddin, S. O. Salawu, and K. Zaimi. "Numerical simulation for the steady nanofluid boundary layer flow over a moving plate with suction and heat generation." SN Applied Sciences 3 (2021): 1-11.
24. Dagan, G. "Some aspects of heat and mass transfer in porous media." In Developments in Soil Science, vol. 2, pp. 55-64. Elsevier, 1972.
25. Trevisan, Osvair V., and Adrian Bejan. "Natural convection with combined heat and mass transfer buoyancy effects in a porous medium." International Journal of Heat and Mass Transfer 28, no. 8 (1985): 1597-1611.

26. Das, S. S., A. Satapathy, J. K. Das, and J. P. Panda. "Mass transfer effects on MHD flow and heat transfer past a vertical porous plate through a porous medium under oscillatory suction and heat source." International journal of heat and mass transfer 52, no. 25-26 (2009): 5962-5969.
27. Sharma, P. R., and Gurminder Singh. "Unsteady MHD free convective flow and heat transfer along a vertical porous plate with variable suction and internal heat generation." International Journal of Applied Mathematics and Mechanics 4, no. 5 (2008): 1-8.
28. Ravikumar, V., M. C. Raju, and G. S. S. Raju. "Heat and mass transfer effects on MHD flow of viscous fluid through non-homogeneous porous medium in presence of temperature dependent heat source." Int J Contemp Math Sci 7, no. 32 (2012): 1597-604.
29. Raju, M. C., C. Veeresh, S. V. K. Varma, K. B. Rushi, and K. A. G. Vijaya. "Heat and mass transfer in MHD mixed convection flow on a moving inclined porous plate." J Appl Comput Math 4, no. 5 (2015): 1-7.
30. Manglesh, Aarti, and M. G. Gorla. "MHD free convective flow through porous medium in the presence of hall current, radiation and thermal diffusion." Indian Journal of Pure and Applied Mathematics 44 (2013): 743-756.
31. Mopuri, Obulesu, Charankumar Ganteda, Bhagyashree Mahanta, and Giulio Lorenzini. "MHD heat and mass transfer steady flow of a convective fluid through a porous plate in the presence of multiple parameters." Journal of Advanced Research in Fluid Mechanics and Thermal Sciences 89, no. 2 (2022): 56-75.
32. Hassani, M., M. Mohammad Tabar, H. Nemati, G. Domairry, and F. Noori. "An analytical solution for boundary layer flow of a nanofluid past a stretching sheet." International Journal of Thermal Sciences 50, no. 11 (2011): 2256-2263.
33. Makinde, Oluwole D., and Abdul Aziz. "Boundary layer flow of a nanofluid past a stretching sheet with a convective boundary condition." International Journal of Thermal Sciences 50, no. 7 (2011): 1326-1332.
34. Abdul-Kahar, Rosmila, and R. Kandasamy. "Scaling group transformation for boundary-layer flow of a nanofluid past a porous vertical stretching surface in the presence of chemical reaction with heat radiation." Computers & Fluids 52 (2011): 15-21.

Nomenclature					
(u, v)	:	velocity components in the (x, y) directions	σ	:	electric conductivity
v	:	kinematic viscosity	μ	:	dynamic viscosity
g	:	acceleration due to gravity	β_T	:	thermal expansion coefficient
ρ	:	fluid density	C	:	concentration of the fluid
T	:	fluid temperature	D_m	:	coefficient of the mass diffusivity
Q_0	:	variable heat source/ generation coefficient	βc	:	concentration expansion coefficient
Q	:	heat generation or absorption term	B_o	:	variable magnetic field

M	:	magnetic field parameter	k	:	thermal conductivity of the fluid
Gr		local Grashof number	Kr	:	chemical reaction parameter
Gc	:	modified local Grashof number	$V(x)$	:	suction/injection parameter
σ*	:	Stefan–Boltzmann constant	k*	:	mean absorption coefficient
j	:	Microinertia density	γ^*	:	Spin gradient velocity
N^*	:	Angular velocity	h	:	Dimensionless angular velocity
T_∞	:	ambient fluid temperature	C_∞	:	ambient fluid concentration
fw	:	Suction/Injection	U_0	:	fluid velocity
Pr	:	Prandtl number	R	:	radiation parameter
Ec	:	Eckert number	Q	:	heat source parameter
Le	:	Lewis Number	Nb	:	Brownian motion parameter
Q	:	radiation absorption coefficient	Nt	:	Thermo-Phoresies parameter
Re_x		Local Reynolds number			